Synthesizing Environmental, Social, and Urban Density Metrics to Predict Urban Heat Island Dynamics using Remote Sensing and Support Vector Regression

Tarranita Kusumadewi
Environmental Science, University of Brawijaya, Malang, Indonesia | Department of Architecture, State Islamic University of Malang, Malang, Indonesia
tarra_nita@arch.uin-malang.ac.id (corresponding author)

Surjono Surjono
Department of Urban and Regional Planning, Faculty of Engineering and Centre of Environmental Studies, University of Brawijaya, Indonesia
surjono@ub.ac.id

Amin Setyo Leksono
Department of Biology, Faculty of Mathematics and Natural Science, University of Brawijaya, Indonesia
aminleksono72@gmail.com

Salma Ainur Rohma
Department of Informatics Engineering, Universitas Islam Negeri Maulana Malik Ibrahim, Malang, Indonesia
200605110007@student.uin-malang.ac.id

Sofia Amalia Husna
Alumnus Department of Architecture, State Islamic University of Malang, Malang, Indonesia
amaliaxofia@gmail.com

Ahmad Fahmi Karami
Department of Informatics Engineering, Universitas Islam Negeri Maulana Malik Ibrahim, Malang, Indonesia | Department of Electrical Engineering, Universitas Islam Negeri Maulana Malik Ibrahim, Malang, Indonesia
afkarami@uin-malang.ac.id

Yunifa Miftachul Arif
Department of Informatics Engineering, Universitas Islam Negeri Maulana Malik Ibrahim, Malang, Indonesia | Department of Electrical Engineering, Universitas Islam Negeri Maulana Malik Ibrahim, Malang, Indonesia
yunif4@ti.uin-malang.ac.id

Received: 1 December 2024 | Revised: 22 February 2025 and 22 March 2025 | Accepted: 2 April 2025

 HTTPS://DOI.ORG/https://doi.org/10.48084/etasr.9791

ABSTRACT

Complex interactions between environmental, social, and urban density factors drive Urban Heat Island (UHI) dynamics. The current study synthesizes multidimensional metrics, including normalized difference indices, such as vegetation (NDVI), water (NDWI), moisture (NDMI), and social parameters (population density), such as urban morphology metrics (UDI) and built-up index (NDBI) to predict UHI intensity using remote sensing data and Support Vector Regression (SVR). Landsat-8, Sentinel-2A, and NASA-SRTM data from 2014 to 2023 were used to analyze Land Surface Temperature (LST) trends and spatially identify UHI hotspots in Malang City, Indonesia. The SVR model demonstrated robust performance, achieving an R^2 of 0.78, an RMSE of 0.23, and a MAPE of 0.46%. Results indicate that increasing urban density (UDI and NDBI) and population density significantly amplify LST, while higher NDVI values mitigate UHI effects. Temporal and spatial analyses reveal a steady expansion of UHI hotspots from central districts (e.g. Klojen) to peripheral areas (e.g. Sukun and Kedungkandang), driven by vegetation loss and urban sprawl. These findings underscore the potential of synthesizing multidimensional metrics for UHI prediction and highlight the value of integrating remote sensing data with machine learning models. The study provides actionable insights for urban planners to design targeted interventions, such as urban greening and density management, to mitigate UHI effects and enhance urban sustainability.

Keywords-UHI; normalized difference indices; environmental indices; multidimensional metrics; remote sensing; SVR; land surface temperature; urban density

I. INTRODUCTION

Broad urbanization has driven unprecedented infrastructure development, significantly altering natural landscapes and intensifying local climate change [1]. One of the most critical outcomes of this transformation is the Urban Heat Island (UHI) phenomenon, where cities experience elevated temperatures compared to their rural surroundings [2]. This phenomenon is primarily caused by anthropogenic activities, reduced vegetation cover, increased impervious surfaces, and dense urban morphology and may exacerbate issues such as heat stress, chronic diseases, rising energy demand, threatened biodiversity, and declining urban livability, especially in rapidly urbanizing areas [3, 4]. Its impact is further magnified in the context of global climate change, necessitating urgent and effective mitigation strategies. Addressing UHI is central to designing climate-resilient cities, particularly in regions experiencing rapid urbanization. Recent studies emphasize the importance of incorporating multidimensional metrics—environmental, urban morphology, and social variables—to model UHI dynamics accurately. For instance, environmental indicators such as the Normalized Difference Vegetation Index (NDVI), Normalized Difference Water Index (NDWI), and Normalized Difference Moisture Index (NDMI) highlight the role of vegetation, water content, and surface moisture in mitigating UHI effects through evapotranspiration and shading [5, 6]. Conversely, urban morphology metrics, including the Urban Density Index (UDI) and the Normalized Difference Built-up Index (NDBI), reveal how impervious surfaces and dense urban structures exacerbate UHI by retaining heat more effectively than natural land cover [7]. Moreover, social factors like population density contribute to anthropogenic heat emissions and energy consumption, further intensifying UHI [8].

Land Surface Temperature (LST) acts as a leading indicator to measure the combined impact of urban environmental, social and morphological variables on UHI. NDVI has a negative relationship with LST because areas with high NDVI values, such as forests and urban parks, tend to be cooler due to the effective evapotranspiration processes and natural shading [9]. In contrast, NDWI and NDMI indicate the ability of water and surface moisture to absorb heat and reduce temperature, so they have a negative relationship with LST [10]. NDBI and UDI, on the other hand, have a strong positive relationship with LST, as areas with high NDBI and UDI values, such as impervious surfaces and dense buildings, tend to absorb and store more heat, which increases surface temperature [11]. In addition, high population density increases anthropogenic activities, such as energy consumption and transport, which further strengthens the positive effect on LST [8]. These direct and indirect relationships suggest that the integration of multidimensional indicators is essential to understanding the spatial and temporal patterns of UHI holistically.

In urban climate research, LST serves as a key metric for assessing UHI. Remote sensing techniques provide an efficient means of measuring LST across spatial and temporal scales. Satellites such as Landsat 8 OLI/TIRS, MODIS, ASTER, and Sentinel-3 SLSTR offer thermal and spectral imagery at varying resolutions, enabling detailed analysis of UHI patterns [12]. The acquired datasets allow researchers to monitor LST trends over time and evaluate the impact of urbanization on local climates. Additionally, Support Vector Regression (SVR) has been used to predict UHI intensity. SVR, derived from Support Vector Machines (SVM), performs regression by mapping data into a higher-dimensional feature space and focusing on a subset of training data (support vectors) to minimize error within a defined margin. Its use of the kernel trick enables efficient handling of complex, non-linear datasets while preventing overfitting, making it an ideal choice for environmental modeling [13]. However, there is a significant research gap regarding the integration of these multidimensional variables in UHI analysis in urban areas with specific contexts, such as tropical climate, diverse topography, and rapid urbanization. Previous research has largely focused on subtropical regions or developed countries with more homogeneous climates [14, 15]. In addition, studies in tropical regions, such as Indonesia, are often limited to using single-scale data without integrating social, environmental, and urban morphological variables simultaneously. This lack of approach may result in UHI analyses that are not comprehensive and less relevant for local data-driven interventions.

Malang City, Indonesia, offers a compelling case study for exploring UHI dynamics. As a mid-sized urban center undergoing rapid urbanization, the city is characterized by diverse topography, a tropical monsoon climate, and significant temperature increases over the past decade, since theaverage temperatures have risen by 1.5 °C. These factors make Malang particularly vulnerable to the adverse effects of UHI, including reduced livability and intensified heat stress. Despite this, a limited number of studies have systematically analyzed UHI dynamics in Malang using an integrated approach that combines environmental, urban morphology, and social metrics.

This study addresses this gap by synthesizing multidimensional variables to model UHI dynamics in Malang City from 2014 to 2023. This research aims to analyze spatial and temporal LST trends, identify key contributing factors, and propose actionable mitigation strategies. The intellectual significance of this study lies in its contribution to the ongoing discourse on the urban environment by emphasizing the complex role of UHI metric variables and uncovering their multifaceted implications across various disciplines. Therefore, this study offers information for targeted interventions, such as urban greening, density management, and climate-sensitive urban design, ultimately contributing to a more sustainable and climate-resilient urban development in Malang City, so the policy makers can develop urban planning strategies that can address the challenges posed by climate change.

II. STUDY AREA

Malang City is located in East Java Province, Indonesia (7.06-8.02 LU 112.06 – 112.07 E). Malang City the second largest city in East Java, with an area of 145.28 km^2 with population density reaching 7627 people per km^2. Malang has geographical characteristics, located in the highlands at an altitude between 440-667 DPL. Malang has a tropical monsoon climate (Köppen climate grouping: Am) with rain and drought seasons. Based on 10 year temperature data observations (2014-2023), Malang City has a cool climate with average temperature variations ranging from 23-29 ^{0}C, as shown in Figure 2.

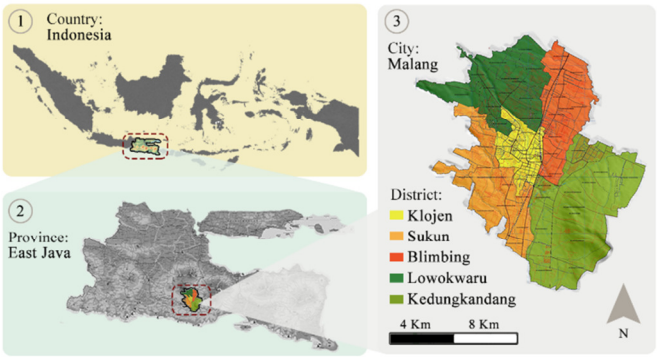

Fig. 1. Location maps of the study area.

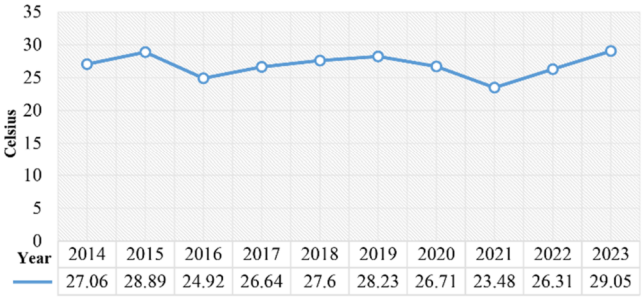

Fig. 2. Ten-year Malang City average temperature.

III. MATERIALS AND METHODS

This study collected all cloud-free data from the Google Earth Engine (GEE) site between 2014 and 2023 to achieve a more accurate picture of the LST. Continuous temperature fluctuations and seasonal changes make studies based on isolated dates less representative. The differences in dates are frequently related to the temporal resolution of the Landsat 8 (16 days) and Sentinel-2A (5 days) satellites. Table 1 describes the Landsat dates and the equivalent Sentinel dates, except that the Shuttle Radar Topography Mission (SRTM) utilizes NASA data from 2000.

TABLE I. SATELITE DATA SOURCES

Time and date	GEE sensor platform	BAND	Variable	Resolution
Every 16 days	Landsat-8 OLI/TIRS C2 L1	ST B10	Surface temperature	100 m
Every 5 days	Sentinel 2A	B3,B4, B8, B11, B12	Vegetation, Building, Water, Moisture	10 m
-	NASA SRTM		Elevation	30 m

The methodology in this study follows a systematic approach divided into four main stages: data collection, data preprocessing, machine learning processing, and data presentation. The first stage, i.e. data collection, involves collecting cloud-free satellite data from various sources such as Landsat 8, Sentinel-2, and SRTM, as explained above. In the data preprocessing phase, data cleaning, normalization, and feature extraction are applied. In the machine learning processing stage, the SVR method is used to predict LST, with a focus on hyperparameter optimization to produce the most accurate predictions. SVR is very effective in modeling non-linear relationships that exist in temperature data, especially in urban areas such as Malang City. The model is tuned with cost, epsilon, gamma, and degree hyperparameters. The cost parameter regulates the trade-off between model complexity and accuracy, ensuring that the model does not overfit. Epsilon defines the tolerance margin for error, providing flexibility in prediction, which is very important in dealing with noisy data. Gamma affects the sensitivity of the model to data points, with higher values making the model more complex, while lower values increase generalization ability. The degree parameter, which is only relevant for polynomial kernels, controls the flexibility of the model by controlling the degree of the polynomial function. The SVR model was evaluated with three

kernels, namely linear, polynomial, and Radial Basis Function (RBF). The linear kernel is used when the relationship between variables is expected to be linear. The polynomial kernel captures more complex patterns by mapping the data to a higher-dimensional space. The RBF kernel is best suited for highly non-linear relationships, making it ideal for LST prediction in urban environments. The combination of these kernels with optimized hyperparameter patterns yields a robust model for LST prediction and analyzing UHI mitigation strategies and helps decision makers formulate more effective plans. Finally, in the data presentation stage, the results of the best-performing model are presented to map and analyze the distribution of UHI in Malang City. All the methodology processes are shown in Figure 3.

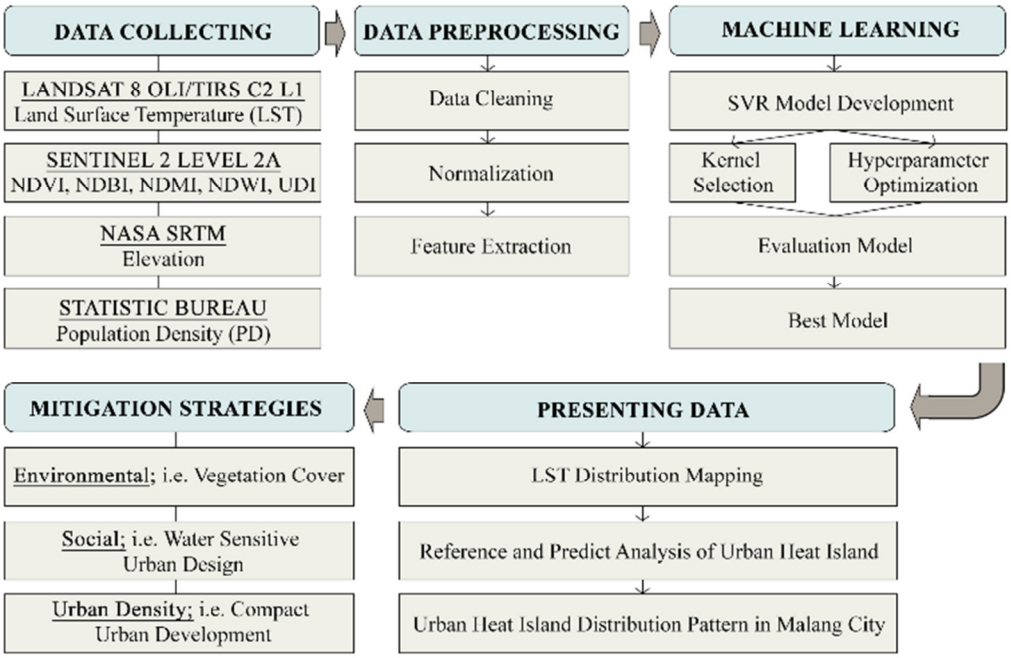

Fig. 3. The procedure flowchart.

A. *LST Data Collection for Environmental Metrics*

The LST data were obtained from the Landsat-8 imagery for two purposes: as a basis for the target attribute (average LST) and as the ground truth for validation (reference LST). Temperature data were obtained from the Landsat 8 OLI/TIRS satellite collection 2, level 1 through the Earth Explorer (https://earthexplorer.usgs.gov/) website as Digital Numbers (DNs). An LST plugin was developed to extract LST from thermal images, primarily using band 10 (Thermal Infrared—TIR sensors) with a spatial resolution of 30 m. Landsat 8 includes two TIR bands, but we recommend using only band 10 for extracting LSTs due to the calibration uncertainty in band 11 from USGS 2019. This plugin converts DNs to radiance and then converts them to brightness temperature values. Furthermore, this plugin uses the red and near-infrared bands (bands 4 and 5, respectively) to calculate the NDVI used in calculating surface emissivity. Finally, the plugin estimates the surface temperature displayed to ^{o}C [16].

The process from DN to radiance is explained below. $L\lambda$ is the radiance corresponding to the Top-of-Atmosphere (ToA) energy in W/(m² sr μm), m_l and a_l are band-specific scale factors (multiplicative and additives) available in metadata, $Qcal$ is the pixel value of the image in DN, and Oi is the calibration at band-10 recommended by the USGS (2019) with a value of -0.29.

$$L\lambda = m_l \times Qcal + a_l - Oi \quad (1)$$

Next, we convert the radiance into brightness temperature. $Tsen$ is the brightness temperature, r is the radiance, and K_a and K_b are band-specific thermal conversion constants:

$$Tsen = \frac{K_a}{ln(\frac{K_b}{r}+1)} \quad (2)$$

We calculate emissivity using NDVI in (5), where ε_v and ε_s are the emissivity of vegetation and soil, respectively, P_v is the proportion of vegetation, and C is a value that refers to the effect of surface geometry.

$$\varepsilon = \varepsilon_v \times P_v + \varepsilon_s \times (1 - P_v) + C \quad (3)$$

LST is calculated in K using Planck's function (4). Ts is the temperature of the land surface, T_b is the temperature of brightness, λ is the wavelength of radiation emitted, ρ is a constant equal to 1.438×10^{-2} mK, and ε is emissivity. The temperature in K is converted to ^{o}C by reducing the value by 273.15 [25].

$$Ts = \frac{T_b}{\{1+[\frac{\lambda T_b}{\rho}]\cdot ln(\varepsilon)\}} \quad (4)$$

Sentinel-2 Level-2A imagery does not require atmospheric correction, as this step has already been completed during image processing. The algorithm, developed by DLR/Telespazio, converts ToA reflectance to Bottom-of-Atmosphere (BoA) reflectance. Sentinel-2 provides 13 spectral bands with spatial resolutions of 10, 20, and 60 m and a 12-bit radiometric resolution. After data collection, we calculate environmental variables, deriving certain features from the collected data. Bands 3, 4, 8, 11, and 12 from the Sentinel-2 satellite correspond to q_1, q_2, q_3, s_1, and s_2, respectively. The features we calculate are the NDVI, NDBI, NDWI, and NDMI.

$$\text{NDVI} = (q_3 - q_2)/(q_3 + q_2) \quad (5)$$

$$\text{NDBI} = (s_2 - q_3)/(s_2 + q_3) \quad (6)$$

$$\text{NDWI} = (q_1 - q_3)/(q_1 + q_3) \quad (7)$$

$$\text{NDMI} = (q_3 - s_1)/(q_3 + s_1) \quad (8)$$

B. Urban Density Data Collection

In addition to the above environmental factors, the urban density variable is used to measure UHI. We use UDI as a parameter. UDI is obtained from the median Built-Up (BU) value defined by:

$$\text{BU} = \text{NDBI} > -0.5 \quad (9)$$

After the BU value is obtained, the UDI value is sought by determining the mean of BU with a value range between -1 to 1, with the following equation:

$$\text{UDI} = \text{NDBI} > -0.5\ \text{NBR} \leq 0.2\ \text{NDWI} \leq 0 \quad (10)$$

C. Population and Elevation Data Collection

Population density in Malang City has experienced a significant increase over the past 10 years. As one of the centers of education and tourism, the city attracts migration of residents from various regions, impacting population growth and population density. We used population density data from Malang Statistic Berau (2014-2023), as shown in Figure 4. Furthermore, the elevation variable was taken from the NASA SRTM map as an input parameter for UHI calculation. The Earth's natural surface elevation remains consistent and does not experience significant changes, even with urbanization. However, elevation will help identify areas exposed to UHI. The elevation data are shown in Figure 5.

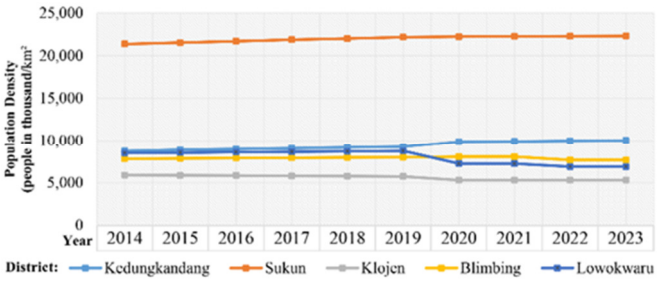

Fig. 4. Malang population district density from 2014 to 2023.

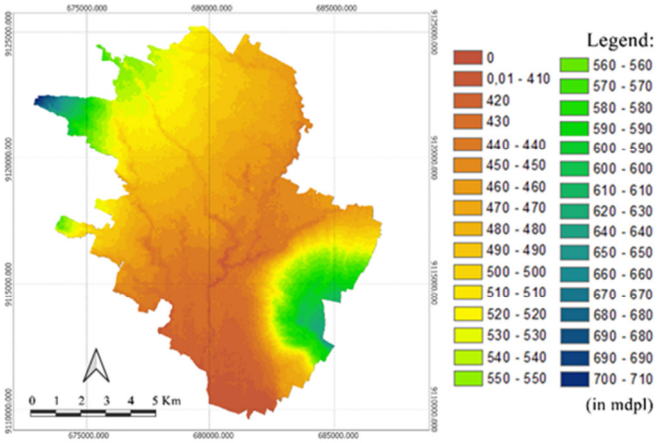

Fig. 5. Elevation data of malang city.

D. SVR Model

Once all the prepared data were ready, data normalization was performed before applying the SVR model. Normalization process used the normalized Z-score to equalize the range of data for each variable:

$$x' = \frac{(x - \mu)}{\sigma} \quad (11)$$

where x is the original value, μ is the mean, and σ is the standard deviation. This normalization process ensures that the data used before being applied to the SVR algorithm have a balanced scale so that the model can predict Environmental Surface heat Gain (ESG) values more accurately.

Once the data have a balanced scale, they are applied to the SVR algorithm for model formation using the RBF kernel. We chose the RBF kernel for its flexibility in handling non-linear relationships between input and output variables. This kernel can map data into higher-dimensional spaces where we can identify linear relationships.

$$y = \sum_{i=1}^{n} (\alpha_i - \alpha_i^*)\, K(x_i, x_j) \quad (12)$$

where y is the prediction output, α_i and α_i^* are model parameters, b is the bias, and $K(x_i, x_j)$ is a kernel function that measures the similarity between two x_i and x_j data points as in (12).

$$K(x_i, x_i) = X_i - X_j \quad (13)$$

$$K(x_i, x_i) = (X_i - X_j + c)^d \quad (14)$$

$$K(x_i, x_i) = exp(\frac{||X_i - X_j||^2}{2\sigma^2}) \quad (15)$$

For the linear kernel, the kernel function is much simpler and is defined as the dot product of the two input vectors in (13). This kernel assumes a linear relationship between the input features, and it works well when the data follow a linear pattern. For the polynomial kernel, the kernel function is defined as (14), where c is a constant, and it is the degree of the polynomial. The degree parameter d controls the flexibility of the kernel by determining the power to which the inner product of X_i and X_j is raised. As the degree increases, the kernel becomes more flexible and capable of capturing higher-order

relationships between data points. For the RBF kernel, the kernel function is defined as (15). $||X_i - X_j||^2$ is the square of the Euclidean distance between two points, and σ is a scale parameter that controls the width of the kernel function. The exponential function ensures the kernel values are within the range (0, 1), where 1 indicates identical data points and a value close to 0 indicates a significant difference. Cost parameter value of 10, epsilon value 0.1, and gamma value 1 were used. Parameter C controls the trade-off between error minimization and model regulation to avoid overfitting. We do not calculate the prediction error based on the epsilon sigma parameter that determines the margin around the hyperplane. The gamma parameter determines how far the influence of a single point data spreads. We then evaluated performance by comparing the actual LST data with the LST prediction results using R^2 and MAPE. R^2 measures how well independent variables explain variation in dependent variables [15]. R^2 values close to 1 indicate an excellent model in explaining data variability. In contrast, MAPE aims to indicate the mean error percentage, which helps understand how much prediction error is in percentage units [17].

IV. RESULTS AND DISCUSSION

From the temporal analysis of data from 2014, 2018, and 2023, we observed significant surface UHI over Malang City as a study area. The indicators include environmental and urban morphology metrics, i.e. NDVI, NDBI, NDWI, NDMI, and UDI as shown in Table II. Over the observed period, this increase in area in LST reflects the intensifying UHI effect, likely driven by ongoing urbanization and changes in land use. The existing UHI area has become widespread and shown a consistent upward trend, increasing from 2014 to 2023, as shown in Figure 6.

TABLE II. MIN AND MAX VALUES OF THE VARIABLES IN 2014, 2018, AND 2023

Variable	Values	Year		
		2014	2018	2023
NDVI	Min	-0.012	0.001	0.016
	Max	0.869	0.882	0.830
	Mean	0.501	0.467	0.421
NDBI	Min	-0.74	-0.753	-0.715
	Max	0.341	0.372	0.360
	Mean	-0.305	-0.258	-0.205
NDWI	Min	-0.794	-0.803	-0.761
	Max	0.01	0.062	0.083
	Mean	-0.493	-0.469	-0.423
NDMI	Min	-0.296	-0.321	-0.316
	Max	0.458	0.486	0.472
	Mean	0.121	0.091	0.055
UDI	Min	0	0	0
	Max	1.02	1.14	1.2
	Mean	0.507	0.571	0.633

After the environmental indicator metric data and urban density are obtained, then social metric data in the form of population density and elevation, as shown in Figures 3 and 4 entered UHI prediction. All these variable metrics were considered as inputs for the regression model. We did not include other variables that might be parameters of the metric variabless because the variables that have been used are the core variables. SVR was employed to predict LST, with 189 tests conducted to fine-tune the model. Hyperparameters—Cost, Epsilon, Gamma, and Degree—were optimized, and three kernels (linear, polynomial, and RBF) were evaluated to capture varying complexities in the data. The Cost parameter balanced model accuracy and complexity, Epsilon allowed for error tolerance, and Gamma controlled sensitivity to data points. The Degree parameter applied only to the polynomial kernel, adjusted model flexibility. This thorough testing enabled the identification of the best configuration for accurate LST predictions and UHI analysis. Meanwhile, the graphic of the SVR Model is shown in Figure 6, and UHI visualization based on actual and SVR models is shown in Figure 7.

The SVR model demonstrated strong predictive capabilities in modeling LST using multidimensional metrics. The model achieved an R^2 of 0.78, an MSE of 0.23, and a MAPE of 0.46%, highlighting its accuracy and robustness. The SVR has been found effective for predicting environmental variables due to its capability to model non-linear relationships, which is critical in complex urban environments [18].

TABLE III. R^2, MAPE, AND MSE VALUES

Kernel	R^2	MAPE	MSE
Linier	0.783	0.445%	0.228
Polynomial	-0.490	1.117%	1.576
RBF	0.809	0.444%	0.202

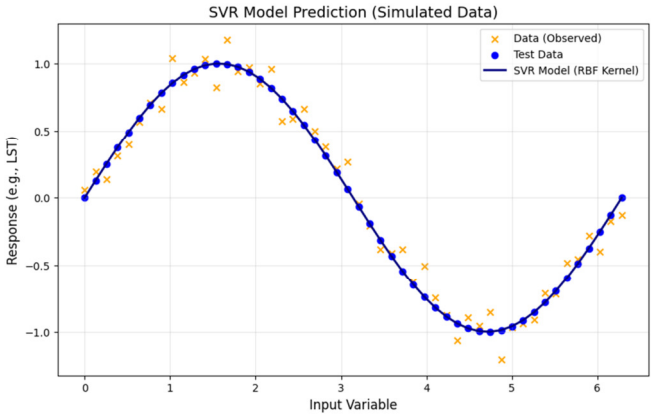

Fig. 6. The graphic of the SVR model.

UDI and NDBI were identified as the strongest positive predictors of LST, emphasizing the impact of impervious surfaces and dense urban structures in intensifying UHI. This is consistent with previous findings. There are similar contributions of NDBI to LST in urban settings [13]. NDVI, on the other hand, showed a significant negative correlation with LST, underscoring the cooling effect of vegetation. This result also aligns with a previous study on the importance of green infrastructure in reducing UHI intensity [19]. Population density is also moderately correlated with LST, reflecting the role of anthropogenic heat emissions. The average LST rose from 23.05°C in 2014 to 28.31°C in 2023, with an intermediate value of 25.14°C in 2018. The results indicate that the LST has increased steadily from 2014 to 2023, reflecting the intensifying UHI effect. Similar studies of upward trends in

built-up indices (NDBI and UDI) point towards continued urban expansion and declining NDVI values, suggesting a loss of green cover [20]. Simultaneously, the NDVI declined from 0.501 to 0.421, indicating substantial vegetation loss (Table II). This finding is consistent with [21], in which it is suggested that the increasing urban footprint and reduction of green spaces are primary factors that exacerbate UHI. Spatially, UHI hotspots expanded outward from central districts like Klojen to suburban areas such as Sukun and Kedungkandang. These districts exhibited the largest increases in NDBI and UDI, corroborating other studies, which identified urban density as a significant driver of UHI intensity [22, 23].

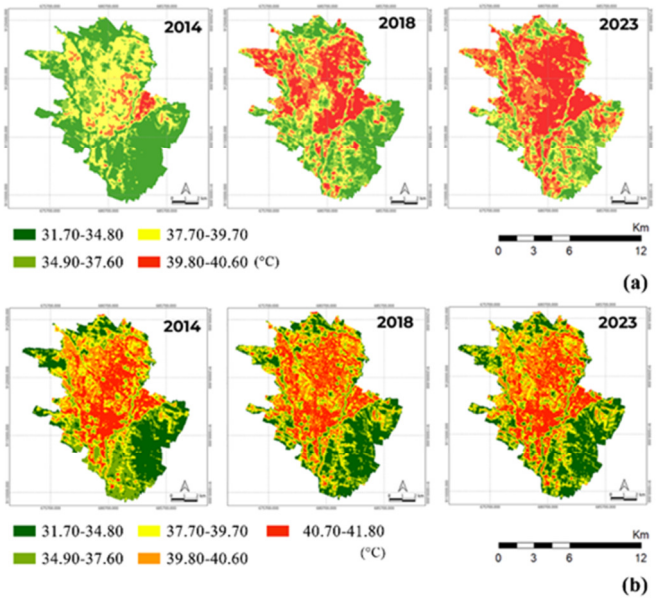

Fig. 7. (a) Actual UHI and (b) predicted UHI by the SVR model.

The study highlights the value of integrating multidimensional metrics for a comprehensive understanding of UHI dynamics. The SVR model effectively synthesized environmental, social, and urban density variables, capturing complex, non-linear relationships between predictors and LST. This approach aligns with other studies that emphasize the utility of machine learning techniques in urban climate studies [24]. The SVR is also known as the best performance prediction model [25].

Regarding the spatial distribution on the 2023 prediction map, the expansion of the medium to the high-temperature zone is spread from the city center to the suburbs. The development and growth of Malang City spread towards the suburbs (southeast to south), namely Sukun and Kedungkandang districts. Based on Malang Statistic Berau data, there has been an increase in density from 8.32 thousand people/km² to 10.04 thousand people/km² in Kedungkandang and from 8.66 thousand people/km² to 9.44 thousand people/km² in Sukun. This condition will have an impact on increasing local temperatures as land transformation for residential and commercial uses reduces green spaces and increases impervious surfaces. Strategies like increasing vegetation cover, implementing water-sensitive urban designs, and promoting compact urban development are critical for mitigating UHI effects [26]. Similar recommendations have been proposed for the role of urban density and vegetation in UHI mitigation in Tehran Province [27].

While the SVR model demonstrated strong performance, there are opportunities for improvement. Incorporating additional variables, such as building heights, energy consumption, and air pollution indices, could enhance the model's predictive accuracy. Furthermore, combining SVR with deep learning techniques, such as Convolutional Neural Networks (CNNs), could improve spatial pattern detection and generalizability [28]. Future research should explore these directions to refine the predictive modeling of UHI and inform climate-resilient urban planning. This study provides actionable insights for urban policymakers and planners in Malang City, demonstrating the potential of integrating multidimensional metrics with machine learning. Also, UHI effects can be mitigated by implementing targeted urban greening based on vegetation loss data, enforcing maximum building density regulations, and adopting reflective materials in urban construction. Strategic urban zoning to manage population density, especially in rapidly growing districts like Sukun and Kedungkandang, alongside integrating green infrastructure with Water-Sensitive Urban Design (WSUD) and incentivizing community-based mitigation actions, are also essential to enhance urban sustainability and climate resilience.

V. CONCLUSION

This study demonstrates the value of synthesizing environmental, social, and urban morphology metrics to predict UHI dynamics in Malang City using remote sensing data and SVR. The findings reveal a steady intensification of UHI effects between 2014 and 2023, driven by urban expansion, vegetation loss, and increased population density. These dynamics were captured effectively by the integration of multidimensional metrics such as NDVI, NDWI, NDMI, UDI, NDBI, and population density. The SVR model showed robust predictive capabilities, achieving an R^2 of 0.809 and a MAPE of 0.44%, highlighting its effectiveness in handling non-linear relationships and diverse variables.

The results showed that urban density metrics (UDI and NDBI) were the strongest contributors to increasing LST. At the same time, NDVI served as a critical mitigating factor, reducing LST through natural cooling mechanisms. The expansion of UHI hotspots from central districts, such as Klojen, to peripheral areas like Sukun and Kedungkandang underscores the compounding effects of urbanization on LST. These findings align with the broader literature, emphasizing the role of urban density and vegetation in shaping UHI intensity. By leveraging remote sensing data and advanced machine learning techniques, this study bridges a critical gap in UHI research, providing a comprehensive framework for analyzing complex urban climate dynamics. The synthesis of environmental, social, and urban metrics offers actionable insights for urban planners and policymakers. Methodologically, this research can be applied to other cities because they have the same type of metric variables. Strategies such as urban greening, water-sensitive urban design, and

density management are essential for mitigating UHI effects and enhancing urban resilience.

This research advances the understanding of UHI by integrating diverse metrics into a predictive framework. It demonstrates the potential of combining remote sensing data with machine learning models like SVR to develop data-driven strategies for climate-resilient urban development. Future research should explore the inclusion of additional variables, such as energy use and air quality, to further enhance predictive accuracy and applicability in various urban contexts.

REFERENCES

[1] Y. Qian *et al.*, "Urbanization Impact on Regional Climate and Extreme Weather: Current Understanding, Uncertainties, and Future Research Directions," *Advances in Atmospheric Sciences*, vol. 39, no. 6, pp. 819–860, Jun. 2022, https://doi.org/10.1007/s00376-021-1371-9.

[2] I. D. Stewart and T. R. Oke, "Local Climate Zones for Urban Temperature Studies," *Bulletin of the American Meteorological Society*, vol. 93, no. 12, pp. 1879–1900, Dec. 2012, https://doi.org/10.1175/BAMS-D-11-00019.1.

[3] K. V. Wong, A. Paddon, and A. Jimenez, "Review of World Urban Heat Islands: Many Linked to Increased Mortality," Journal of Energy Resource Technology, vol. 135, no. 2, Jun. 2013, Art. no. 022101, https://doi.org/10.1115/1.4023176.

[4] H. Li *et al.*, "A new method to quantify surface urban heat island intensity," *Science of The Total Environment*, vol. 624, pp. 262–272, May 2018, https://doi.org/10.1016/j.scitotenv.2017.11.360.

[5] H. Ren, "An Overview of Land Surface Temperature Retrieval from Chinese Gaofen-5 Thermal Infrared Images," in *IGARSS 2019 - 2019 IEEE International Geoscience and Remote Sensing Symposium*, Yokohama, Japan, Jul. 2019, pp. 150–153, https://doi.org/10.1109/IGARSS.2019.8899816.

[6] X. Luan *et al.*, "Remote Sensing and Social Sensing Data Reveal Scale-Dependent and System-Specific Strengths of Urban Heat Island Determinants," *Remote Sensing*, vol. 12, no. 3, Jan. 2020, Art. no. 391, https://doi.org/10.3390/rs12030391.

[7] C. Yuan, A. S. Adelia, S. Mei, W. He, X.-X. Li, and L. Norford, "Mitigating intensity of urban heat island by better understanding on urban morphology and anthropogenic heat dispersion," *Building and Environment*, vol. 176, Jun. 2020, Art. no. 106876, https://doi.org/10.1016/j.buildenv.2020.106876.

[8] H. Li, S. Sodoudi, J. Liu, and W. Tao, "Temporal variation of urban aerosol pollution island and its relationship with urban heat island," *Atmospheric Research*, vol. 241, Sep. 2020, Art. no. 104957, https://doi.org/10.1016/j.atmosres.2020.104957.

[9] A. Yadav, R. Kumar, and S. Swarup, "Remote Sensing Image-Based Analysis of the Urban Heat Island Effect in Relation to the Normalized Difference Vegetation Index (NDVI): A Case Study of Patna Municipal Corporation," *International Journal for Research in Applied Science & Engineering Technology*, vol. 11, no. 1, pp. 1142–1155, Jan. 2023, https://doi.org/10.22214/ijraset.2023.48777.

[10] P. C. Chanyal and S. Purohit, "A Geospatial analysis of Climate Change Impacts: Relationship of Normalized Difference Water Index (NDWI and Land Surface Temperature (LST) in Kumaun Himalaya," Research Square, Jul. 22, 2024, https://doi.org/10.21203/rs.3.rs-4490692/v1.

[11] M. Cetin, M. Ozenen Kavlak, M. A. Senyel Kurkcuoglu, G. Bilge Ozturk, S. N. Cabuk, and A. Cabuk, "Determination of land surface temperature and urban heat island effects with remote sensing capabilities: the case of Kayseri, Türkiye," *Natural Hazards*, vol. 120, no. 6, pp. 5509–5536, Apr. 2024, https://doi.org/10.1007/s11069-024-06431-5.

[12] H. P. U. Fonseka, H. Zhang, Y. Sun, H. Su, H. Lin, and Y. Lin, "Urbanization and Its Impacts on Land Surface Temperature in Colombo Metropolitan Area, Sri Lanka, from 1988 to 2016," *Remote Sensors*, vol. 11, no. 8, Apr. 2019, Art. no. 957, https://doi.org/10.3390/rs11080957.

[13] A. Mathew, S. Sreekumar, S. Khandelwal, and R. Kumar, "Prediction of land surface temperatures for surface urban heat island assessment over Chandigarh city using support vector regression model," *Solar Energy*, vol. 186, pp. 404–415, Jul. 2019, https://doi.org/10.1016/j.solener.2019.04.001.

[14] Y. Liu, T. Li, and H. Peng, "A new structure of permeable pavement for mitigating urban heat island," *Science of The Total Environment*, vol. 634, pp. 1119–1125, Sep. 2018, https://doi.org/10.1016/j.scitotenv.2018.04.041.

[15] Q. Xie and Q. Sun, "Monitoring thermal environment deterioration and its dynamic response to urban expansion in Wuhan, China," *Urban Climate*, vol. 39, Sep. 2021, Art. no. 100932, https://doi.org/10.1016/j.uclim.2021.100932.

[16] M. Isaya Ndossi and U. Avdan, "Application of Open Source Coding Technologies in the Production of Land Surface Temperature (LST) Maps from Landsat: A PyQGIS Plugin," *Remote Sensors*, vol. 8, no. 5, May 2016, Art. no. 413, https://doi.org/10.3390/rs8050413.

[17] K. H. Suradiradja, I. S. Sitanggang, L. Abdullah, and I. Hermadi, "Estimation of biomass of forage sorghum (sorghum bicolor) Cv. Samurai-2 using support vector regression," vol. 30, no. 3, pp. 1786–1794, Jun. 2023, https://doi.org/10.11591/ijeecs.v30.i3.pp1786-1794.

[18] M. Varentsov, M. Krinitskiy, and V. Stepanenko, "Machine Learning for Simulation of Urban Heat Island Dynamics Based on Large-Scale Meteorological Conditions," *Climate*, vol. 11, no. 10, Oct. 2023, Art. no. 200, https://doi.org/10.3390/cli11100200.

[19] M. Pena Acosta, F. Vahdatikhaki, J. Santos, A. Hammad, and A. G. Dorée, "How to bring UHI to the urban planning table? A data-driven modeling approach," *Sustainable Cities and Society*, vol. 71, Aug. 2021, Art. no. 102948, https://doi.org/10.1016/j.scs.2021.102948.

[20] P. Tian *et al.*, "Assessing spatiotemporal characteristics of urban heat islands from the perspective of an urban expansion and green infrastructure," *Sustainable Cities and Society*, vol. 74, Nov. 2021, Art. no. 103208, https://doi.org/10.1016/j.scs.2021.103208.

[21] D. Erdem Okumus and F. Terzi, "Evaluating the role of urban fabric on surface urban heat island: The case of Istanbul," *Sustainable Cities and Society*, vol. 73, Oct. 2021, Art. no. 103128, https://doi.org/10.1016/j.scs.2021.103128.

[22] C. Wang, H. Zhang, Z. Ma, H. Yang, and W. Jia, "Urban Morphology Influencing the Urban Heat Island in the High-Density City of Xi'an Based on the Local Climate Zone," *Sustainability*, vol. 16, no. 10, May 2024, Art. no. 3946, https://doi.org/10.3390/su16103946.

[23] T. He *et al.*, "Quantifying the effects of urban development intensity on the surface urban heat island across building climate zones," *Applied Geography*, vol. 158, Sep. 2023, Art. no. 103052, https://doi.org/10.1016/j.apgeog.2023.103052.

[24] Y. Sun, C. Gao, J. Li, R. Wang, and J. Liu, "Quantifying the Effects of Urban Form on Land Surface Temperature in Subtropical High-Density Urban Areas Using Machine Learning," *Remote Sensors*, vol. 11, no. 8, Apr. 2019, Art. no. 959, https://doi.org/10.3390/rs11080959.

[25] M. Ali, I. Ullah, W. Noor, A. Sajid, A. Basit, and J. Baber, "Predicting the Session of an P2P IPTV User through Support Vector Regression (SVR)," *Engineering, Technology & Applied Science Research*, vol. 10, no. 4, pp. 6021–6026, Aug. 2020, https://doi.org/10.48084/etasr.3635.

[26] T. Kusumadewi, S. Surjono, A. S. Leksono, and Y. M. Arif, "Exploring neighborhood green space to mitigate UHI effect based on a spatial approach in Malang, Indonesia," *IOP Conference Series: Earth and Environmental Science*, vol. 1312, Oct. 2024, Art. no. 012008, https://doi.org/10.1088/1755-1315/1312/1/012008.

[27] A. Zarei, R. Shah-Hosseini, S. Ranjbar, and M. Hasanlou, "Validation of non-linear split window algorithm for land surface temperature estimation using Sentinel-3 satellite imagery: Case study; Tehran Province, Iran," *Advances in Space Research*, vol. 67, no. 12, pp. 3979–3993, Jun. 2021, https://doi.org/10.1016/j.asr.2021.02.019.

[28] G. Suthar, N. Kaul, S. Khandelwal, and S. Singh, "Predicting land surface temperature and examining its relationship with air pollution and urban parameters in Bengaluru: A machine learning approach," *Urban Climate*, vol. 53, Jan. 2024, Art. no. 101830, https://doi.org/10.1016/j.uclim.2024.101830.